International Journal of Precision Engineering and Manufacturing (2024) 25:995–1010
https://doi.org/10.1007/s12541-024-00966-0

Online ISSN 2005-4602
Print ISSN 2234-7593

REGULAR PAPER

Adaptive Identification of the Position-independent Geometric Errors for the Rotary Axis of Five-axis Machine Tools to Directly Improve Workpiece Geometric Errors

Seung-Han Yang[1] · Kwang-Il Lee[2]

Received: 3 October 2023 / Revised: 15 January 2024 / Accepted: 16 January 2024 / Published online: 17 February 2024

Abstract
Identification of, and compensation for, geometric errors is a cost-effective way to reduce the volumetric errors of five-axis machine tools and thus reduce workpiece geometric errors. An adaptive identification method is introduced to directly reduce workpiece geometric errors. We determined the relation between the root-sum-square values of geometric error sensitivity coefficients and workpiece geometric errors. Then, an optimal measurement path minimizing those values was adaptively determined to identify position-independent geometric errors of the rotary axis. We applied our method to improve the radial deviation of the cone-shaped ISO 10791-7 testpiece, as an example. The radial deviations were 22.6 and 27.6 µm in the counterclockwise (CCW) and clockwise (CW) directions, respectively, after compensating for the position-independent geometric errors identified using a common measurement path. These values improved by 27% and 17% to 16.4 and 22.9 µm in the CCW and CW directions, respectively, after compensating for the position-independent geometric errors identified using the optimal measurement path, thus confirming the validity of our approach.

Keywords Adaptive identification · Position-independent geometric error · Measurement uncertainty · Sensitivity coefficient · Workpiece geometric error

List of symbols

b	Setting angle of a ball on the workpiece table, degrees
n_A	Sample number of A-axis measurements, µm
n_C	Sample number of C-axis measurements, µm
n_W	Sample number along the workpiece toolpath, µm
o_{ij}	Offset error of the j-axis relative to the i-direction $(i = x, y, z; \quad j = a, c)$, µm
s_{ij}	Squareness error of the j-axis around the i-direction $(i = x, y, z; \quad j = a, c)$, µrad
R	Nominal radius of a circular measurement path for the A-axis, mm
$\Delta R_{i,j,k}$	k-Th deviation in the j-direction of the i-axis $(i = A, C; \quad j = radial, axial;$ $k = 1, \ldots, n_A$ for A - axis; $k = 1, \ldots, n_C$ for C - axis$)$, µm
$(x_{M,i}, y_{M,i}, z_{M,i})$	Measured positional deviations $\left(i = 1, \ldots, n_A\right.$ for A - axis; $\left.i = 1, \ldots, n_C\right.$ for C - axis$)$, µm
$(x_{W,i}, y_{W,i}, z_{W,i}, a_{W,i}, c_{W,i})$	iTh workpiece coordinate $\left(i = 1, \ldots, n_W\right)$
$(x_{TP,i}, y_{TP,i}, z_{TP,i}, a_{TP,i}, c_{TP,i})$	Toolpath command corresponding to the ith workpiece coordinate $\left(i = 1, \ldots, n_W\right)$

✉ Kwang-Il Lee
kilee@kiu.kr

Seung-Han Yang
syang@knu.ac.kr

[1] School of Mechanical Engineering, Kyungpook National University, 80, Daehak-ro, Buk-gu, Daegu 41566, Republic of Korea

[2] School of Mechanical and Automotive Engineering, Kyungil University, 50, Gamasil-gil, Hayang-eup, Gyeongsan-si, Gyeongbuk 38428, Republic of Korea

$\left(\Delta x_W, \Delta y_W, \Delta z_W\right)$	Set-up error of a ball on the workpiece table, µm
$\{\mathbf{i}\}$	Coordinate system of the i-axis $\{i = X, Y, Z, A, C\}$
$\{\mathbf{R}\}, \{\mathbf{W}\}, \{\mathbf{t}\}$	Coordinate system of the reference, workpiece, and tool, respectively
$\mathbf{VE}_i\left(x_{VE,i}, y_{VE,i}, z_{VE,i}\right)$	Volumetric errors at the ith toolpath command $\left(i = 1, \ldots, n_W\right)$
$\boldsymbol{\tau}_i^j$	4×4 Homogeneous transformation matrix from the j to i coordinate system

1 Introduction

The volumetric errors of machine tools decrease when geometric errors are identified and compensated, in turn reducing kinematic [1], stiffness-induced [2], and thermally induced [3] errors. Geometric errors can be identified via direct and indirect methods [4, 5]. Geometric errors are divided into position-independent geometric errors (PIGEs; also termed "location and orientation errors" [6] and "kinematic errors" [7]) and position-dependent geometric errors (PDGEs; also termed "error motions" [8]). PIGEs are defined using the averages of the PDGEs over the working range of linear and rotary axes, and thus affect volumetric error more significantly across the entire workspace [9]. Thirteen PIGEs are used to model the volumetric errors of five-axis machine tools, including three squareness errors between the three linear axes; two squareness errors and two offset errors for the rotary and tilting axes, respectively; and two squareness errors for the spindle axis [10, 11]. Although several methods of PIGE identification are available [6], it remains challenging to accurately determine the PIGEs of rotary axes; no method is optimal for identifying the errors.

PIGEs must be accurately identified to reduce workpiece geometric errors. However, PDGEs affect PIGEs because they are coupled. Thus, it is important to check the interdependencies of PIGEs and PDGEs, and to perform Monte Carlo simulations to investigate the effects of the interdependency [12]. Certain PIGEs are affected by the PDGEs [13], thermal errors [14] of linear axes, and PDGEs of both rotary and linear axes [15]. It is necessary to pre-identify and pre-compensate for PDGEs that affect rotary-axis PIGEs. However, this makes PIGE identification complex. Alternatively, as recommended here, PIGE identification can be optimized to minimize the effects of other errors (including PDGEs) on PIGEs.

Geometric errors affect workpiece geometric errors. The effects of PIGEs [7], and of PIGEs and PDGEs [16], on the machining geometric accuracy of a cone frustum have been investigated; the workpiece geometric errors were determined via simultaneous control of all five axes [17]. A cubic machining test was used to reveal the effects of geometric errors on the workpiece coordinate system [18]. A pyramidal testpiece was machined in a five-axis machine tool and measured using a coordinate measuring machine (CMM) to identify PIGEs alone [19], and both PIGEs and PDGEs [20, 21]. Three machining patterns were used, and CMM measurements were obtained; 11 PIGEs were identified on a single drive of a rotary axis and unwanted effects on the most sensitive direction were reduced, thereby enhancing accurate identification [22]. A cubic workpiece was subjected to five machining patterns via several large rotations of the rotary axes; a laser displacement sensor was employed to measure finished surface mismatches [23]. However, PIGEs identified via machining tests can be affected by errors in workpiece settings, cutting force, and tool parameters, which reduce the accuracy of the identified PIGEs [18]. Methods not affected by such errors have thus been developed. PIGEs are systematic deviations identified via double ball-bar (DBB) measurements of the eccentricity of three-axis circular motions [24]. An R-test using a device measuring three relative displacements has been applied to identify PIGEs after inducing circular-spherical movements [25]. DBB measurements on a single set-up have also been employed to identify PIGEs; down-time was reduced when the structural restrictions of machine tools were considered [26, 27]. To simplify measurements, one method identified PIGEs via single-axis control during a series of DBB measurements [28]. A DBB method with a single setup, single-axis control, and extension bar was used to identify PIGEs [29]. A reconfigurable mechanism model was employed to identify the PIGEs of machine tools using arbitrary combinations of linear and rotary axes [30]. All of the above methods are single-ball measurements derived using a DBB or the R-test device; in principle, a touch-trigger probe could also be employed. Other methods derive multi-ball [31] and square column measurements using a touch-trigger probe [32] to identify PIGEs. However, single-ball methods have the advantages of a simple set-up and cost-effective measurement; ISO standards employ such measurements [33]. Geometric errors are identified by optimizing the distribution of measurement points to reduce volumetric errors [34]. However, there are no optimized methods for workpiece geometric errors [24, 25, 33].

It is essential to consider the measurement uncertainties of identified PIGEs, where these uncertainties reflect a lack of precise knowledge of the measurand values [35]. In general, PIGEs are the sums of sensitivity coefficients multiplied by the measured data [9]. The sensitivity coefficients describe how output estimates vary as the input estimates change [36, 37]. During PIGE identification, the root-sum-square (RSS) values of sensitivity coefficients, which are affected by the measuring angle range for rotary axes, are used to determine the measurement conditions [38]; uncertainties in measured data are induced by both measuring devices and systematic and non-systematic errors of the controlled axes [32]. Measurement uncertainty can be improved by reducing the RSS values of the sensitivity coefficients and/or uncertainties in the measured data. However, such reduction of the measured data requires highly accurate (and thus expensive) measuring devices. Pre-measurement of other systematic errors should be performed using additional devices, again increasing costs. It is reasonable to seek to optimize measurement paths by reducing the effects of the RSS values of sensitivity coefficients on workpiece geometric errors; this is a cost-effective approach.

In summary, the PIGEs of rotary axes are identified using a number of methods to improve the volumetric errors of five-axis machine tools, and measurement uncertainties are analyzed via error budgeting; this reveals the confidence intervals of the PIGEs and the feasibility of the chosen methods. However, all methods to date have aimed to improve machine tool volumetric errors, rather than to directly improve workpiece geometric errors (Fig. 1a); the improvement is thus limited.

Here, we developed an adaptive method for identifying the PIGEs of rotary axes; this directly improves workpiece geometric errors (Fig. 1b) by optimizing the measurement processes. The processes are adaptively optimized for the workpiece rather than the machine tools. The measurement processes are optimized by determining the measurement paths that minimize the effects of PIGE sensitivity coefficients on workpiece geometric errors, whereas our previous method [38] used PIGE sensitivity coefficients to determine the measuring angle range for rotary axes without considering workpiece geometric errors. The method proposed in this study is shown in Fig. 2.

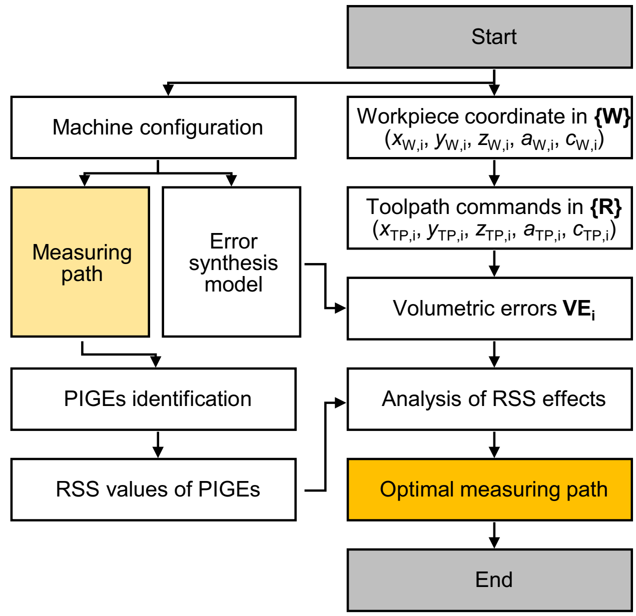

Fig. 2 Adaptive method for identifying the PIGEs of rotary axes

First, a workpiece coordinate $\left(x_{W,i}, y_{W,i}, z_{W,i}, a_{W,i}, c_{W,i}\right)$ $\left(i = 1, \ldots, n_W\right)$ in the workpiece coordinate system $\{\mathbf{W}\}$ is assigned, and toolpath commands

Fig. 1 Strategies used to improve workpiece accuracy

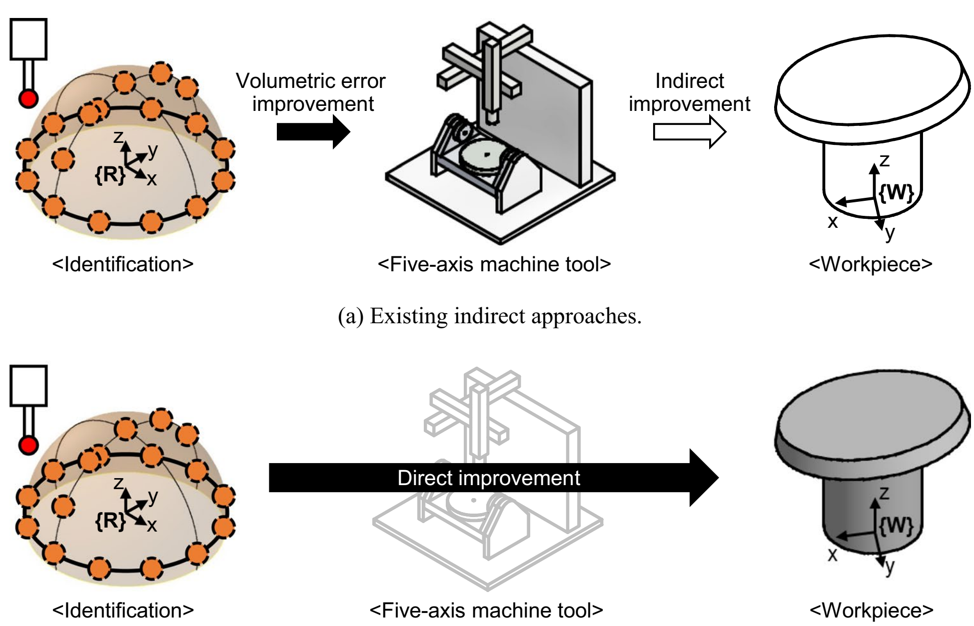

(a) Existing indirect approaches.

(b) Our direct approach.

$\left(x_{TP,i}, y_{TP,i}, z_{TP,i}, a_{TP,i}, c_{TP,i}\right)$ $\left(i = 1, \ldots, n_W\right)$ in a reference coordinate system $\{\mathbf{R}\}$ are calculated for five-axis control. Then, the volumetric errors $\mathbf{VE}_i\left(i = 1, \ldots, n_W\right)$ for the toolpath commands are derived as functions of the commands and PIGEs, using an error synthesis model determined by the experimental machine configuration. The effects of the PIGE RSS values (which are affected by the measurement path) on workpiece geometric errors are analyzed, and an optimal path is determined to minimize such effects. In Sect. 2, a measurement path model concerned with the RSS values of the PIGE sensitivity coefficients is optimized for the cone-shaped ISO 10791–7, M3_15 testpiece [17]. We use this example because this is a representative workpiece that requires simultaneous five-axis control. We then identify the PIGEs using a R-test device. Equivalent DBB measurements (with PIGE compensation) are also performed, and demonstrate the validity of our approach based on the improvement in cone-shaped testpiece radial deviation (Sect. 3). The main contributions of this study are discussed in Sect. 4.

2 Optimal measurement path for workpiece geometric errors

2.1 Error synthesis model

To identify PIGEs, it is essential to establish an error synthesis model as a function of the nominal commands for the linear and rotary axes. Then, the relationships between the measured data and PIGEs are established using the model. The kinematic structure of our experimental machine tool is shown in Fig. 3 and the PIGEs of the rotary axes are listed in Table 1.

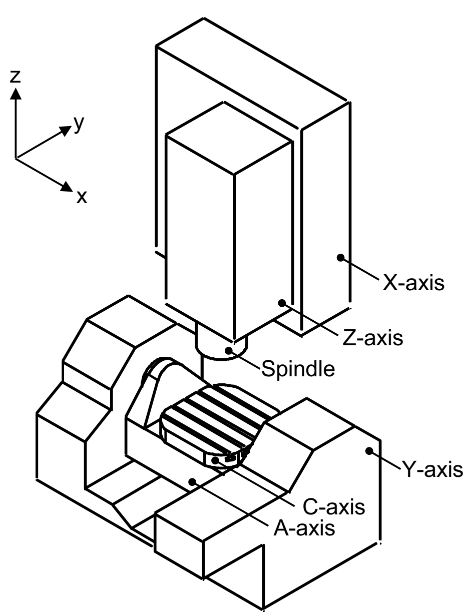

Fig. 3 Kinematic structure of the experimental machine tool

Table 1 PIGEs of the rotary axes of the experimental five-axis machine tool

Axis	PIGEs	Location and orientation errors (ISO 230–1)	Unit
A	o_{ya}	E_{Y0A}	μm
	o_{za}	E_{Z0A}	μm
	s_{ya}	E_{B0A}	μrad
	s_{za}	E_{C0A}	μrad
C	o_{xc}	E_{X0C}	μm
	o_{yc}	E_{Y0C}	μm
	s_{xc}	E_{A0C}	μrad
	s_{yc}	E_{B0C}	μrad

PIGE: position-independent geometric error

To identify the PIGEs, the ball positions on the workpiece table and tool nose are described using the homogeneous transformation matrices of Eq. (1). Here, $\left(x_{TP,i}, y_{TP,i}, z_{TP,i}, a_{TP,i}, c_{TP,i}\right)$ $\left(i = 1, \ldots, n_W\right)$ are the i-th toolpath commands corresponding to workpiece coordinate $\left(x_{W,i}, y_{W,i}, z_{W,i}, a_{W,i}, c_{W,i}\right)$ $\left(i = 1, \ldots, n_W\right)$. The terms $ca_{TP,i}$, $sa_{TP,i}$, $cc_{TP,i}$, and $sc_{TP,i}$ are cos $\left(a_{TP,i}\right)$, sin $\left(a_{TP,i}\right)$, cos $\left(c_{TP,i}\right)$, and sin $\left(c_{TP,i}\right)$, respectively. The reference coordinate system $\{\mathbf{R}\}$ is defined at the nominal crosspoint of rotary axes A and C; this allows for a simple description of the volumetric errors.

$$\begin{aligned}\boldsymbol{\tau}_R^w &= \boldsymbol{\tau}_R^Y\boldsymbol{\tau}_Y^A\boldsymbol{\tau}_A^C\boldsymbol{\tau}_C^w \\ \boldsymbol{\tau}_R^T &= \boldsymbol{\tau}_R^X\boldsymbol{\tau}_X^Z\boldsymbol{\tau}_Z^T\end{aligned} \tag{1}$$

where:

(for the workpiece branch):

$$\boldsymbol{\tau}_R^Y = \begin{bmatrix} 1 & 0 & 0 & 0 \\ 0 & 1 & 0 & -y_{TP,i} \\ 0 & 0 & 1 & 0 \\ 0 & 0 & 0 & 1 \end{bmatrix},$$

$$\begin{aligned}\boldsymbol{\tau}_Y^A &= \begin{bmatrix} 1 & 0 & 0 & 0 \\ 0 & 1 & 0 & o_{ya} \\ 0 & 0 & 1 & o_{za} \\ 0 & 0 & 0 & 1 \end{bmatrix} \times \begin{bmatrix} 1 & -s_{za} & s_{ya} & 0 \\ s_{za} & 1 & 0 & 0 \\ -s_{ya} & 0 & 1 & 0 \\ 0 & 0 & 0 & 1 \end{bmatrix} \times \begin{bmatrix} 1 & 0 & 0 & 0 \\ 0 & ca_{TP,i} & sa_{TP,i} & 0 \\ 0 & -sa_{TP,i} & ca_{TP,i} & 0 \\ 0 & 0 & 0 & 1 \end{bmatrix} \\ &= \begin{bmatrix} 1 & -s_{za}ca_{TP,i} - s_{ya}sa_{TP,i} & -s_{za}sa_{TP,i} + s_{ya}ca_{TP,i} & 0 \\ s_{za} & ca_{TP,i} & sa_{TP,i} & o_{ya} \\ -s_{ya} & -sa_{TP,i} & ca_{TP,i} & o_{za} \\ 0 & 0 & 0 & 1 \end{bmatrix},\end{aligned}$$

$$\boldsymbol{\tau}_A^C = \begin{bmatrix} 1 & 0 & 0 & o_{xc} \\ 0 & 1 & 0 & o_{yc} \\ 0 & 0 & 1 & 0 \\ 0 & 0 & 0 & 1 \end{bmatrix} \times \begin{bmatrix} 1 & 0 & s_{yc} & 0 \\ 0 & 1 & -s_{xc} & 0 \\ -s_{yc} & s_{xc} & 1 & 0 \\ 0 & 0 & 0 & 1 \end{bmatrix} \times \begin{bmatrix} cc_{TP,i} & sc_{TP,i} & 0 & 0 \\ -sc_{TP,i} & cc_{TP,i} & 0 & 0 \\ 0 & 0 & 1 & 0 \\ 0 & 0 & 0 & 1 \end{bmatrix}$$

$$= \begin{bmatrix} cc_{TP,i} & sc_{TP,i} & s_{yc} & o_{xc} \\ -sc_{TP,i} & cc_{TP,i} & -s_{xc} & o_{yc} \\ -s_{yc}cc_{TP,i} - s_{xc}sc_{TP,i} & -s_{yc}sc_{TP,i} + s_{xc}cc_{TP,i} & 1 & 0 \\ 0 & 0 & 0 & 1 \end{bmatrix},$$

$$\boldsymbol{\tau}_C^w = \begin{bmatrix} x_{W,i} \\ y_{W,i} \\ z_{W,i} \\ 1 \end{bmatrix},$$

$$\boldsymbol{\tau}_Z^T = \begin{bmatrix} 1 & 0 & 0 & 0 \\ 0 & 1 & 0 & 0 \\ 0 & 0 & 1 & 0 \\ 0 & 0 & 0 & 1 \end{bmatrix}$$

The volumetric errors $\mathbf{VE}_i \ (i = 1, \ldots, n_W)$ (positional deviations of the ball on the workpiece table from the nominal values) are defined by Eq. (2). Note that the volumetric errors $\mathbf{VE}_i$ are defined in the reference coordinate system $\{\mathbf{R}\}$, and thus can be used directly to compensate for the identified PIGEs via the G-code modification [39]. Here, $\mathbf{VE}_{coeff,i}$ refers to the sensitivity of the PIGEs to volumetric errors $\mathbf{VE}_i$.

$$\begin{aligned} \begin{bmatrix} \mathbf{VE}_i \\ \hline 0 \end{bmatrix} &= \left(\boldsymbol{\tau}_R^T\right)^{-1} \times \boldsymbol{\tau}_R^w - \left(\boldsymbol{\tau}_R^T\right)^{-1} \times \boldsymbol{\tau}_R^Y \times \mathbf{AM}_A \times \mathbf{AM}_C \times \boldsymbol{\tau}_C^w \\ &= \begin{bmatrix} \left(x_{W,i}sa_{TP,i}sc_{TP,i} + y_{W,i}sa_{TP,i}cc_{TP,i} + z_{W,i}ca_{TP,i}\right)s_{ya} + \left(-x_{W,i}ca_{TP,i}sc_{TP,i} - y_{W,i}ca_{TP,i}cc_{TP,i} + z_{W,i}sa_{TP,i}\right)s_{za} + o_{xc} + z_{W,i}s_{yc} \\ o_{ya} + \left(x_{W,i}cc_{TP,i} - y_{W,i}sc_{TP,i}\right)s_{za} + o_{yc}ca_{TP,i} - \left(x_{W,i}sa_{TP,i}sc_{TP,i} + y_{W,i}sa_{TP,i}cc_{TP,i} + z_{W,i}ca_{TP,i}\right)s_{xc} + \left(x_{W,i}sa_{TP,i}cc_{TP,i} - y_{W,i}sa_{TP,i}sc_{TP,i}\right)s_{yc} \\ o_{za} + \left(-x_{W,i}cc_{TP,i} + y_{W,i}sc_{TP,i}\right)s_{ya} + o_{yc}sa_{TP,i} + \left(x_{W,i}ca_{TP,i}sc_{TP,i} + y_{W,i}ca_{TP,i}cc_{TP,i} - z_{W,i}sa_{TP,i}\right)s_{xc} + \left(-x_{W,i}ca_{TP,i}cc_{TP,i} + y_{W,i}ca_{TP,i}sc_{TP,i}\right)s_{yc} \\ \hline 0 \end{bmatrix} \\ &= \begin{bmatrix} \mathbf{VE}_{coeff,i} \\ \hline 0 \end{bmatrix} \times \mathbf{PIGEs} \end{aligned} \tag{2}$$

(for the tool branch):

$$\boldsymbol{\tau}_R^X = \begin{bmatrix} 1 & 0 & 0 & x_{TP,i} \\ 0 & 1 & 0 & 0 \\ 0 & 0 & 1 & 0 \\ 0 & 0 & 0 & 1 \end{bmatrix},$$

$$\boldsymbol{\tau}_X^Z = \begin{bmatrix} 1 & 0 & 0 & 0 \\ 0 & 1 & 0 & 0 \\ 0 & 0 & 1 & z_{TP,i} \\ 0 & 0 & 0 & 1 \end{bmatrix},$$

where

$$\mathbf{VE}_i = [\, x_{VE,i} \ y_{VE,i} \ z_{VE,i} \,]^T,$$

$$\mathbf{AM}_a = \begin{bmatrix} 1 & 0 & 0 & 0 \\ 0 & ca_{TP,i} & sa_{TP,i} & 0 \\ 0 & -sa_{TP,i} & ca_{TP,i} & 0 \\ 0 & 0 & 0 & 1 \end{bmatrix},$$

$$\mathbf{AM}_c = \begin{bmatrix} cc_{TP,i} & sc_{TP,i} & 0 & 0 \\ -sc_{TP,i} & cc_{TP,i} & 0 & 0 \\ 0 & 0 & 1 & 0 \\ 0 & 0 & 0 & 1 \end{bmatrix},$$

$$\mathbf{VE}_{coeff,i} = \begin{bmatrix} 0 & 1 & 0 \\ 0 & 0 & 1 \\ x_{W,i}sa_{TP,i}sc_{TP,i} + y_{W,i}sa_{TP,i}cc_{TP,i} + z_{W,i}ca_{TP,i} & 0 & -x_{W,i}cc_{TP,i} + y_{W,i}sc_{TP,i} \\ -x_{W,i}ca_{TP,i}sc_{TP,i} - y_{W,i}ca_{TP,i}cc_{TP,i} + z_{W,i}sa_{TP,i} & x_{W,i}cc_{TP,i} - y_{W,i}sc_{TP,i} & 0 \\ 1 & 0 & 0 \\ 0 & ca_{TP,i} & sa_{TP,i} \\ 0 & -x_{W,i}sa_{TP,i}sc_{TP,i} - y_{W,i}sa_{TP,i}cc_{TP,i} - z_{W,i}ca_{TP,i} & x_{W,i}ca_{TP,i}sc_{TP,i} + y_{W,i}ca_{TP,i}cc_{TP,i} - z_{W,i}sa_{TP,i} \\ z_{W,i} & x_{W,i}sa_{TP,i}cc_{TP,i} - y_{W,i}sa_{TP,i}sc_{TP,i} & -x_{W,i}ca_{TP,i}cc_{TP,i} + y_{W,i}ca_{TP,i}sc_{TP,i} \end{bmatrix}$$

$$\mathbf{PIGEs} = \left[\, o_{ya} \ o_{za} \ s_{ya} \ s_{za} \ o_{xc} \ o_{yc} \ s_{xc} \ s_{yc} \,\right]^T$$

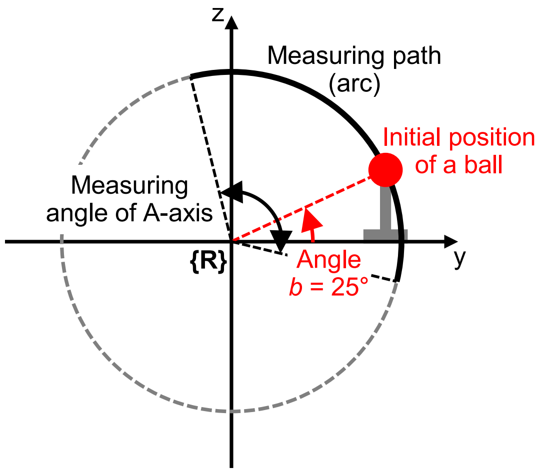

(a) Measurement path with $b = 25°$.

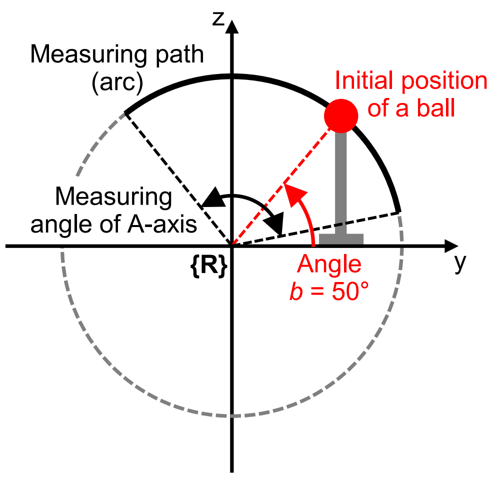

(b) Measurement path with $b = 50°$.

Fig. 4 Measurement paths according to the initial position of the ball on the workpiece table

2.2 General measurement path for PIGEs

Two linear axes and a rotary axis are often controlled to identify PIGEs [33]. For the C-axis, it is easy to measure the positional deviations of the ball on the workpiece table along the full circle trajectory followed by the X, Y, and C axes. Thus, the measurement uncertainties are small. However, for the A-axis, the nominal measuring angle range is limited because the A-axis involves tilting only, i.e., not full rotation. Thus, the measurement path of the ball (followed by the Y, Z, A axes) on the workpiece table is limited to an arc, creating relatively large measurement uncertainties in the PIGEs. The measurement path can be changed in space (Fig. 4) depending on the initial position of the ball on the table, although the measuring angle range does not change. For example, Fig. 4a and b show the different measurement paths when the initial position of a ball on the table is changed. The measurement uncertainties of the PIGEs are affected by the measurement path determined by the initial position of the ball. In this case, the initial position is modeled using setting angle b, which must be optimized to minimize the effects of PIGE sensitivity coefficients on workpiece geometric errors.

In Sect. 3, we measure the positional deviation of the ball on the workpiece table using a wireless Trinity probe (IBS Precision Engineering BV, Eindhoven, The Netherlands). In such a case, the ball position $\left(x_{W,i}, y_{W,i}, z_{W,i}\right)\left(i = 1, \dots, n_W\right)$, which remains the same during measurements, is given by Eq. (3). The set-up error $\left(\Delta x_W, \Delta y_W, \Delta z_W\right)$ is unknown and fixed if the ball installation is not varied, and is used to describe the ball position in coordinate system $\{\mathbf{C}\}$. Here, cb and sb are $\cos(b)$ and $\sin(b)$, respectively. The nominal commands $\left(x_{TP,i}, y_{TP,i}, z_{TP,i}, a_{TP,i}, c_{TP,i}\right)\left(i = 1, \dots, n_W\right)$ for the linear and rotary axes are given by Eq. (4) for the A- and C-axis measurements, respectively. Note that the ball position $\left(x_{W,i}, y_{W,i}, z_{W,i}\right)$ on the workpiece table does not change during measurements with a single set-up.

$$\left(x_{W,i}, y_{W,i}, z_{W,i}\right) = \left(Rcb + \Delta x_W, \Delta y_W, Rsb + \Delta z_W\right) \tag{3}$$

$$\begin{aligned}
&\text{For A - axis} \\
&\begin{cases}
x_{TP,i} = 0 \\
y_{TP,i} = Rc\left(-a_{TP,i} + b\right) \\
z_{TP,i} = Rs\left(-a_{TP,i} + b\right) \\
a_{TP,i} = [a_{\min}, a_{\max}],\ \left(i = 1, \dots, n_A\right) \\
c_{TP,i} = -90°
\end{cases} \\
&\text{For C - axis} \\
&\begin{cases}
x_{TP,i} = Rcbcc_{TP,i} \\
y_{TP,i} = -Rcbsc_{TP,i} \\
z_{TP,i} = Rsb \\
a_{TP,i} = 0° \\
c_{TP,i} = [c_{\min}, c_{\max}],\ \left(i = 1, \dots, n_C\right)
\end{cases}
\end{aligned} \tag{4}$$

By substituting Eqs. (3) and (4) into Eq. (2), the volumetric errors $\mathbf{VE}_i$ are derived (along with the measurement paths) in Cartesian coordinates. However, it is essential to represent volumetric error $\mathbf{VE}_i$ in terms of cylindrical coordinates to minimize the effects of the main PDGEs (i.e., the angular positioning errors) of the rotary axes [38, 40]. In such a case, the relationships between the PIGEs and measured positional deviations $\left(x_{M,i}, y_{M,i}, z_{M,i}\right)$ $\left(i = 1, \dots, n_A \text{ for A - axis}; \quad i = 1, \dots, n_C \text{ for C - axis}\right)$ of the ball along the measurement path, are derived as shown in Eq. (5).

$$
\begin{aligned}
&\text{For A - axis: Radial}\\
&\Delta R_{A,radial,i} = \sqrt{\left(y_{TP,i}+y_{M,i}\right)^2+\left(z_{TP,i}+z_{M,i}\right)^2} - \\
&\quad R = c\left(-a_{TP,i}+b\right)o_{ya} + s\left(-a_{TP,i}+b\right)o_{za} + cbo_{yc} + cb\Delta x_W + sb\Delta z_W\\
&\text{For A - axis: Axial}\\
&\Delta R_{A,axial,i} = x_{M,i} = Rs\left(-a_{TP,i}+b\right)s_{ya} - Rc\left(-a_{TP,i}+b\right)s_{za} + o_{xc} + Rsbs_{yc} - \Delta y_W\\
&\text{For C - axis: Radial}\\
&\Delta R_{C,radial,i} = \sqrt{\left(x_{TP,i}+x_{M,i}\right)^2+\left(y_{TP,i}+y_{M,i}\right)^2} - \\
&\quad Rcb = \left\{o_{xc} + R\left(s_{ya}+s_{yc}\right)sb\right\}cc_{TP,i} - \left\{\left(o_{ya}+o_{yc}\right) - Rsbs_{xc}\right\}sc_{TP,i} + \Delta x_W\\
&\text{For C - axis: Axial}\\
&\Delta R_{C,axial,i} = z_{M,i} = -Rcbsc_{TP,i}s_{xc} - R\left(s_{ya}+s_{yc}\right)cbcc_{TP,i} + o_{za} + \Delta z_W
\end{aligned}
\tag{5}
$$

Equation (5) is formatted using the matrix notation of Eq. (6), and the PIGEs are identified using a least-squares approach at the given angle b. It is obvious that the coefficient matrices $\mathbf{A}_{i,j}$ $(i = A,\ C; j = radial,\ axial)$ are affected by angle b.

$$\mathbf{A}_{i,j}\mathbf{x}_{i,j} = \Delta\mathbf{R}_{i,j} \quad (i = A, C; \quad j = radial, axial) \tag{6}$$

2.3 Optimal measurement path using the RSS values

Pseudo-inversion of Eq. (6) yields Eq. (7). The PIGEs are identified by multiplying the rows of the pseudo-inverse matrix $\mathbf{A}^{+}_{i,j}$ by the measured data $\Delta\mathbf{R}_{i,j}$ [Eq. (8)]. Here, $\Delta R_{i,j,k}$ $\left(i = A, C; \quad j = radial, axial; \quad k = 1, \dots, n_A \text{ for A - axis}; \ k = 1, \dots, n_C \text{ for C - axis}\right)$ refers to the k-th component of the measured data $\Delta\mathbf{R}_{i,j}$ $(i = A, C; j = radial,\ axial)$. Thus, the rows of the pseudo-inverse matrix $\mathbf{A}^{+}_{i,j}$ constitute the set of sensitivity coefficients for the corresponding PIGEs.

$$\mathbf{x}_{i,j} = \left(\mathbf{A}^T_{i,j}\ \mathbf{A}_{i,j}\right)^{-1}\ \mathbf{A}^T_{i,j}\ \Delta\mathbf{R}_{i,j} = \mathbf{A}^{+}_{i,j}\ \Delta\mathbf{R}_{i,j} \tag{7}$$

$$PIGEs = f\left(\Delta R_{i,j,k}\right) = \sum_{i,j,k}\left\{\frac{\partial f}{\partial\left(\Delta R_{i,j,k}\right)}\Delta R_{i,j,k}\right\} \tag{8}$$

Next, the measurement uncertainties of the PIGEs, $U(PIGEs)$, are calculated as the RSS values of the sensitivity coefficients, RSS_{PIGEs}, multiplied by the measurement uncertainties $U\left(\Delta R_{i,j,k}\right)$ [Eq. (9)] [36, 37]. The units for $U(PIGEs)$, $U\left(\Delta R_{i,j,k}\right)$ and RSS_{PIGEs} are summarized in Table 2. Here, it is assumed that the measurement uncertainties $U\left(\Delta R_{i,j,k}\right)$ are identical over the measuring paths in Fig. 4, as the uncertainties are affected by the measuring devices and systematic and non-systematic errors of the controlled axes, as stated in Sect. 1.

Table 2 Measurement uncertainty units for $U(PIGEs)$, $U\left(\Delta R_{i,j,k}\right)$, and the RSS values

Item	Unit	Description
$U(PIGEs)$	µm for offset errors, $\{o_{ya}, o_{za}, o_{xc}, o_{yc}\}$ µrad for squareness errors, $\{s_{ya}, s_{za}, s_{xc}, s_{yc}\}$	Measurement uncertainties for identified PIGEs
$U\left(\Delta R_{i,j,k}\right)$	µm	Measurement uncertainties of measured data $\Delta R_{i,j,k}$
RSS_{PIGEs}	µm/µm for offset errors, $\{o_{ya}, o_{za}, o_{xc}, o_{yc}\}$ µrad/µm for squareness errors, $\{s_{ya}, s_{za}, s_{xc}, s_{yc}\}$	RSS values of the sensitivity coefficients

$$U(PIGEs) = RSS_{PIGEs} \times U\left(\Delta R_{i,j,k}\right) = \sqrt{\sum_{i,j,k} \left\{ \frac{\partial f}{\partial\left(\Delta R_{i,j,k}\right)} \right\}^2} \times U\left(\Delta R_{i,j,k}\right) \tag{9}$$

The measurement uncertainty $U(PIGEs)$ is affected by both RSS_{PIGEs} and measurement uncertainty $U\left(\Delta R_{i,j,k}\right)$. The RSS_{PIGEs} are a function of angle b. To improve workpiece geometric errors directly, it is essential to investigate the effects of measurement uncertainty $U(PIGEs)$ on the measurement uncertainty $U\left(\mathbf{VE}_i\right)$ along the toolpaths $\left(x_{TP,i}, y_{TP,i}, z_{TP,i}, a_{TP,i}, c_{TP,i}\right)$ $\left(i = 1, \ldots, n_W\right)$. The measurement uncertainty $U\left(\mathbf{VE}_i\right)$ is determined as shown in Eq. (10) [using Eq. (2)]. Here, the units for $U\left(\mathbf{VE}_i\right)$ and $RSS_{VE,j,i}$ $(j = x, y, z)$ are µm and µm/µm, respectively.

$$U\left(\mathbf{VE}_i\right) = \begin{bmatrix} U\left(x_{VE,i}\right) \\ U\left(y_{VE,i}\right) \\ U\left(z_{VE,i}\right) \end{bmatrix} = \begin{bmatrix} RSS_{VE,x,i} \\ RSS_{VE,y,i} \\ RSS_{VE,z,i} \end{bmatrix} \times U\left(\Delta R_{j,k,m}\right) \tag{10}$$

where:

$$RSS_{VE,x,i} = \sqrt{\sum_{n=1}^{8} \mathbf{Q}_i^2(1, n)},$$

$$RSS_{VE,y,i} = \sqrt{\sum_{n=1}^{8} \mathbf{Q}_i^2(2, n)},$$

$$RSS_{VE,z,i} = \sqrt{\sum_{n=1}^{8} \mathbf{Q}_i^2(3, n)},$$

$$\mathbf{Q}_i = \mathbf{VE}_{coeff,i} \times \left[RSS_{oya}\ RSS_{oza}\ RSS_{sya}\ RSS_{sza}\ RSS_{oxc}\ RSS_{oyc}\ RSS_{sxc}\ RSS_{syc} \right]^T$$

The measurement uncertainty $U\left(\mathbf{VE}_i\right)\left(i = 1, \ldots, n_W\right)$ is affected by both $RSS_{VE,j,i}\left(i = 1, \ldots, n_W;\quad j = x, y, z\right)$ (which is in turn affected by angle b) and measurement uncertainty $U\left(\Delta R_{j,k,m}\right)$ (which is constant). Thus, the measurement uncertainty $U\left(\mathbf{VE}_i\right)$ can be improved by decreasing $RSS_{VE,j,i}$ $\left(i = 1, \ldots, n_W;\quad j = x, y, z\right)$; this is achieved in a cost-effective manner by determining the optimal angle b. The effect of angle b on $RSS_{VE,j,i}$ along the toolpaths $\left(x_{TP,i}, y_{TP,i}, z_{TP,i}, a_{TP,i}, c_{TP,i}\right)\left(i = 1, \ldots, n_W\right)$ should be minimized for optimal adaptive identification. For example, we explored the effect of angle b on the $RSS_{VE,j,i}$ along toolpaths of the ISO 10791-7 cone-shaped testpiece, and optimized angle b to minimize unwanted effects. The case study is described in Sect. 3.

3 Case study

3.1 Determination of the optimal measurement path

As an example, the optimal angle b is determined for the cone-shaped testpiece of ISO 10791-7, M3_15 [17]; this standard requires simultaneous control of five axes. The testpiece dimensions are shown in Fig. 5 and Table 3. In Sect. 3.3, DBB measurement (equivalent to machining) is performed to measure the radial deviation of the lower surface of the cone without and with PIGE compensation. The testpiece diameter D is 200 mm (not 80 mm in ISO 10791-7 [17]) because the nominal length of the experimental DBB is 100 mm. The spindle axis is constrained to lie tangential to the cone surface, and the toolpaths $\left(x_{TP,i}, y_{TP,i}, z_{TP,i}, a_{TP,i}, c_{TP,i}\right)$ $(i = 1, \ldots, 720)$ according to testpiece angle ψ are calculated as shown in Fig. 6. Here, $n_W = 720$, because the toolpath is calculated as ψ is varied 0°–360° in steps of $\Delta\psi = 0.5°$.

The simulation sequence is summarized in Fig. 7. First, angle b in the range $[0°, 60°]$ with an interval $\Delta b = 5°$ is chosen and RSS_{PIGEs} is calculated using Eq. (9) (Fig. 8). Note that RSS_{PIGEs} varies with angle b. As that increases, the RSS_{PIGEs} for $\left\{o_{ya}, o_{yc}, s_{za}\right\}$ (which reflects the sensitivity in the y-direction) decrease, and the measurement uncertainties of $\left\{o_{ya}, o_{yc}, s_{za}\right\}$ are thus reduced. In contrast, as angle b increases, the RSS_{PIGEs} for $\left\{o_{za}, o_{xc}, s_{ya}, s_{xc}, s_{yc}\right\}$ (which reflect sensitivity in the x- and z-directions) increase, and the measurement uncertainties of $\left\{o_{za}, o_{xc}, s_{ya}, s_{xc}, s_{yc}\right\}$ are thus increased. However, it is not essential to improve the RSS_{PIGEs} of all PIGEs. The reduction of workpiece geometric errors mainly requires an analysis of the effects of RSS_{PIGEs} on the volumetric error $\mathbf{VE}_i$ along testpiece toolpaths. As such, we used small (25°) and large (50°) angles of b to investigate the effect of this angle on volumetric error $\mathbf{VE}_i$ over the cone-shaped testpiece.

$RSS_{VE,i,j}$ $(i = x, y, z;\quad j = 1, \ldots, 720)$ were calculated in Cartesian coordinates using Eq. (10) (Fig. 9a). The $RSS_{VE,i,j}$ vary because the effects of RSS_{PIGEs} on volumetric error $\mathbf{VE}_i$ change with testpiece angle ψ. The peak-to-valley (PV) values of $RSS_{VE,i,j}$ are greater at a large angle of b (50°) than at a small angle (25°).

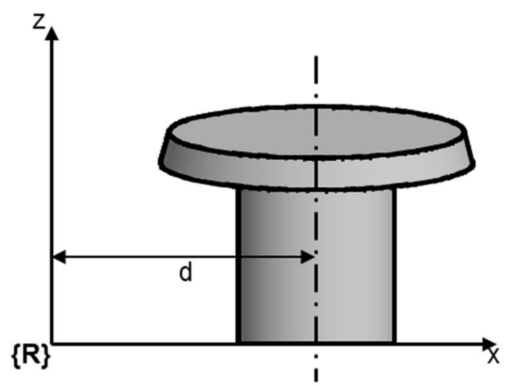

(a) In the ZX plane.

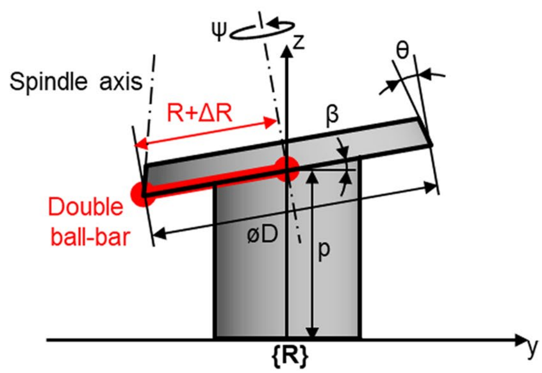

(b) In the YZ plane.

Fig. 5 Cone-shaped testpiece

However, not all $RSS_{VE,i,j}$ affect workpiece geometric errors, including the radial deviation of the cone lower surface; the radial deviations at that surface are critical for evaluating the cone-shaped testpiece because they reflect the lack of precise data on roundness. Thus, $RSS_{VE,i,j}$ $(i = x, y, z;\quad j = 1, \ldots, 720)$ in the Cartesian coordinate system are transformed into a cylindrical coordinate system, i.e., $RSS_{VE,i,j}$ $(i = radial, tangential, axial;\quad j = 1, \ldots, 720)$ (Fig. 9b). This

Table 3 Dimensions of the cone-shaped testpiece

Parameter	Value	Description
d	125 mm	Offset from C-axis
D	200 mm	Diameter of bottom surface
p	116 mm	Offset from A-axis
θ	15°	Half-apex angle
β	10°	Inclination angle
ψ	[0°, 360°]	Testpiece angle

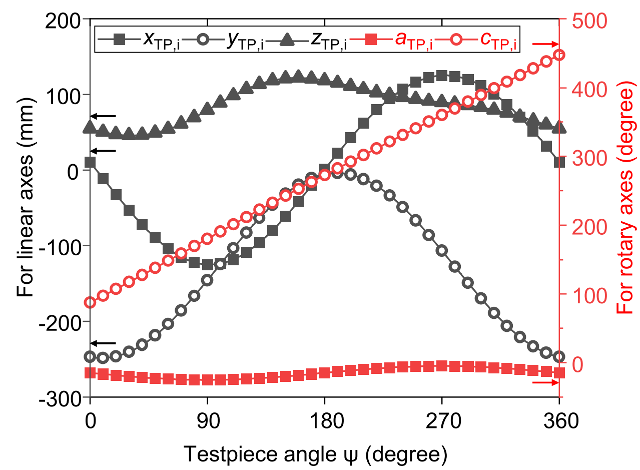

Fig. 6 Toolpath commands for the cone-shaped testpiece

yields PV values of $RSS_{VE,i,j}$ $(i = radial;\quad j = 1, \ldots, 720)$ of 0.3 and 0.2 µm/µm for angles of *b* of 25° and 50°, respectively. This reveals that testpiece radial deviation is further improved (by about 33%) when PIGEs are identified at $b = 50°$ and compensated for, compared to the case when $b = 25°$. To determine the optimal angle *b*, the sum of the $RSS_{VE,i,j}$ $(i = radial;\quad j = 1, \ldots, 720)$ along toolpaths $\left(x_{TP,i}, y_{TP,i}, z_{TP,i}, a_{TP,i}, c_{TP,i}\right)$ $(i = 1, \ldots, 720)$ is calculated as shown in Fig. 10. The sum of the $RSS_{VE,i,j}$ $(i = radial;\quad j = 1, \ldots, 720)$ changes according to angle *b*; the minimum (optimal) value occurs when $b = 50°$. Note that the sum of $RSS_{VE,i,j}$ $(i = tangential, axial;\quad j = 1, \ldots, 720)$ increases with angle *b*, but this does not affect testpiece accuracy.

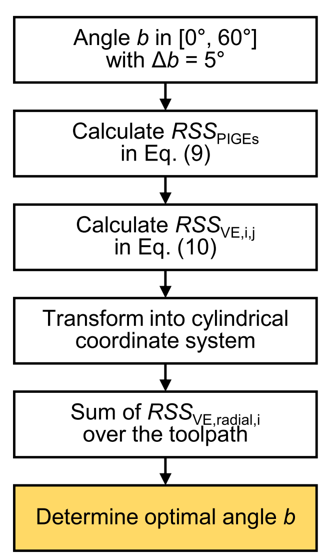

Fig. 7 Simulation sequence to derive the optimal angle *b*

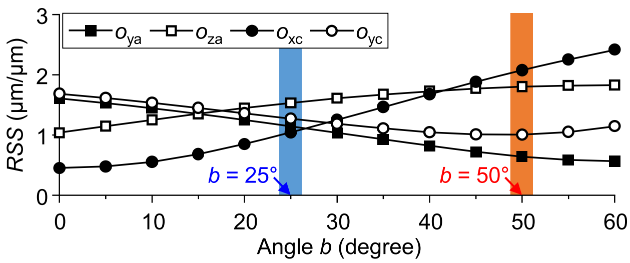

(a) For offset errors

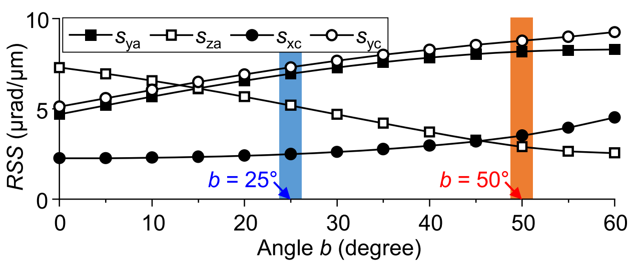

(b) For squareness errors

Fig. 8 Calculated RSS_{PIGEs} by the angle b

3.2 Experiments

3.2.1 PIGE identification according to angle b

The PIGEs of an experimental machine tool (VMD 600/5AX; Doosan Machine Tools Co. Ltd., Republic of Korea) were identified at b angles of 50° (the optimal condition) and 25° using the wireless Trinity probe (Fig. 11). To identify the PIGEs, static data were collected over the range [−90°, 30°] in steps of $\Delta a = 15°$ (sample number $n_A = 9$) for the A-axis, and over the range [0°, 360°] in steps of $\Delta c = 45°$ (sample number $n_C = 9$) for the C-axis.

The positional deviations $\left(x_{M,i}, y_{M,i}, z_{M,i}\right)$ along all measurement paths exhibited large PVs (Fig. 12, in black) because the PIGEs were high. When the deviations $\left(x_{M,i}, y_{M,i}, z_{M,i}\right)$ were inserted into Eqs. (5–8), the PIGEs shown in Fig. 13 were identified. The values differed, which was attributable to the various sensitivity coefficients of Eq. (8) that depend on angle b. By compensating the identified PIGEs using G-code modification, the positional deviations $\left(x_{M,i}, y_{M,i}, z_{M,i}\right)$ were clearly improved at b angles of 25° and 50° (Fig. 12, in red), as was the measurement path. However, this does not guarantee direct improvements in workpiece geometric errors. Thus, we assessed how the PIGEs identified at b angles of 25° and 50° affected such errors.

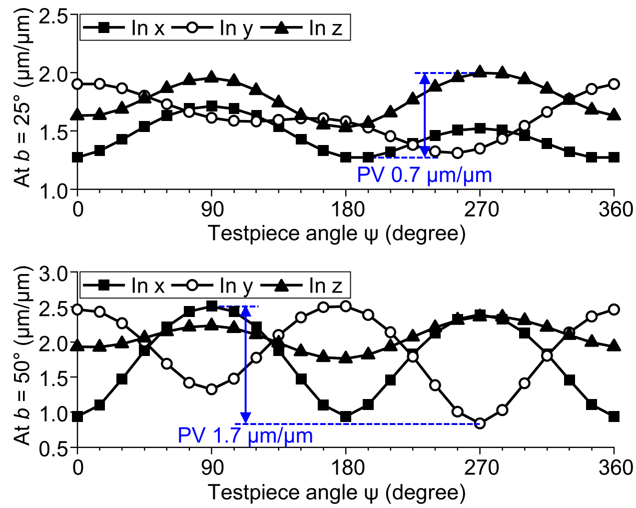

(a) In Cartesian coordinates.

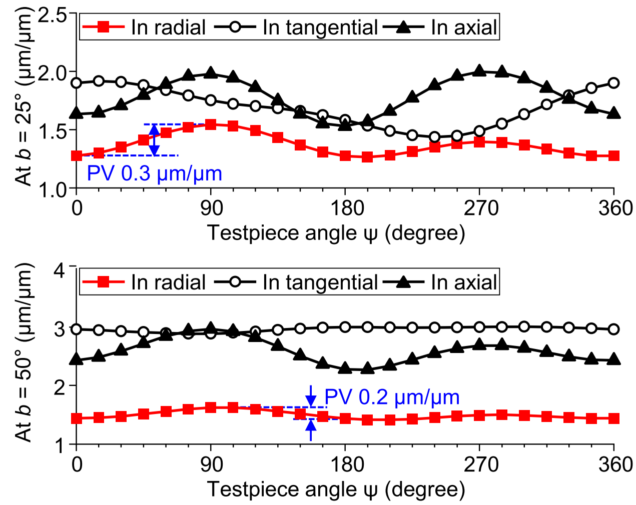

(b) In cylindrical coordinates.

Fig. 9 $RSS_{VE,i,j}$ values at b angles of 25° and 50°

3.2.2 DBB measurement for the cone-shaped testpiece

We performed DBB measurements (equivalent to testpiece machining) to assess the radial deviation of the cone-shaped testpiece (Fig. 14). A DBB (QC20-w; Renishaw plc., Kingswood, UK) was used to measure radial deviations ΔR_i $(i = 1, \ldots, 2132)$ at a nominal length $R = 100$ mm along the bottom circular path of the testpiece without and with compensation of the PIGEs identified at b angles of 25° and 50°. For the DBB measurements, a ball was fixed on the workpiece table and another ball was fixed at the tool nose. Then, the distance between the two balls, along with the measurement path, were measured using a linear-variable-differential-transformer sensor. The ball on the

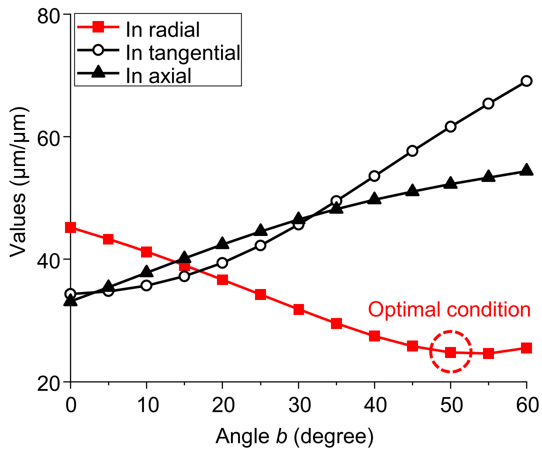

Fig. 10 Sum of $RSS_{VE,i}$ (i = *radial*, *tangential*, *axial*) over the testpiece and the range of angle b

workpiece table deviated from the nominal position in the coordinate system {**C**} due to two main factors: the PIGEs of the machine tool itself [41] and the set-up error caused by imperfection of the clamping device used for the ball.

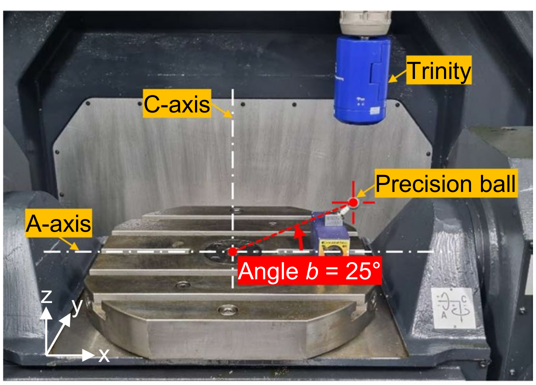

(a) At angle $b = 25°$.

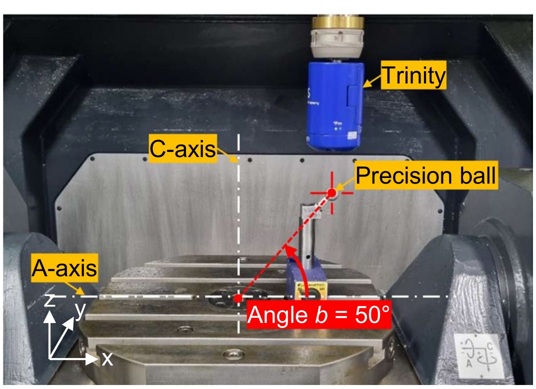

(b) At angle $b = 50°$.

Fig. 11 Experimental set-up for different angles b

However, the set-up error of the experimental clamping device is negligible [42]. The deviation of the ball on the workpiece table was mainly affected by PIGEs and can be further reduced by compensating for the identified PIGEs. Thus, we used the raw measured deviation ΔR_i as the radial deviation, without eliminating the eccentric center of the least squares circle [43], to investigate the PIGE effect for the cone-shaped testpiece.

Without PIGE compensation (Fig. 15), the PV values were large, i.e., 94.8 and 95.5 µm in the counter-clockwise (CCW) and clockwise (CW) directions, respectively. Thus, the DBB measurements were repeated with PIGE compensation (Fig. 13). For angle $b = 25°$ (Fig. 16a, b), in black], the PVs improved to 22.6 and 27.6 µm in the CCW and CW directions, respectively, showing the effectiveness of PIGE identification and compensation. However, this was achieved by improving the volumetric errors of the experimental machine tool, rather than by directly improving the workpiece geometric errors. Thus, the improvements were significant but limited. The PVs with compensation for the identified PIGEs at $b = 50°$ (Fig. 16a, b), in red] were 16.4 and 22.9 µm in the CCW and CW directions, respectively. Thus, the radial deviation values were further improved by 27% and 17%, respectively, after compensating for the identified PIGEs at the optimal angle. Therefore, workpiece geometric errors can be reduced cost-effectively simply by using an optimal angle b, rather than by decreasing the uncertainties of measured data.

4 Summary and conclusion

The rotary axis PIGEs can be identified using the method in ISO 10791-6. However, the method is not optimized to reduce PIGE measurement uncertainties, associated with workpiece geometric errors. Thus, we proposed an adaptive identification method. The measurement paths for adaptive identification of rotary axis PIGEs described in ISO 10791-6 were modeled according to the initial angle of a precision ball installed on a workpiece table. PIGEs were calculated as the sum of the sensitivity coefficients multiplied by the measured deviations, and PIGE measurement uncertainties were defined as the RSS values of the sensitivity coefficients multiplied by the uncertainties of the measured data. The effects of the RSS values on workpiece geometric errors were explored using an error synthesis model. The effect of the summed RSS values on volumetric errors along the workpiece toolpath was calculated and used as the criterion for the optimal initial angle. Finally, PIGEs were identified using an optimized measurement path to reduce workpiece geometric errors. The main findings of our study are as follows:

Fig. 12 Measured positional deviations without/with compensation

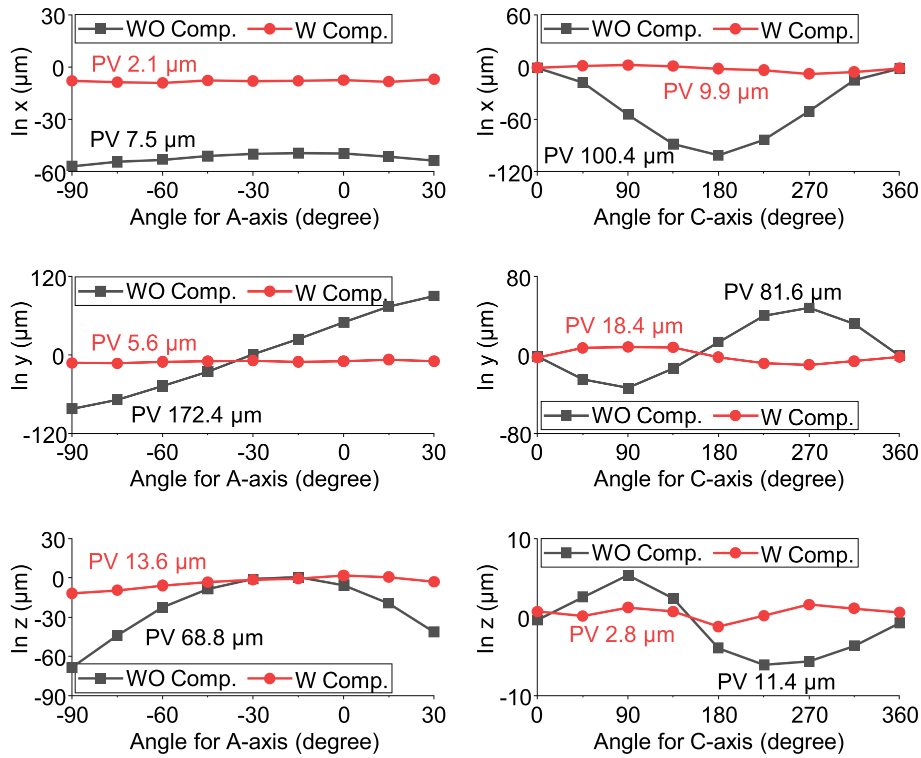

(a) At angle $b = 25°$.

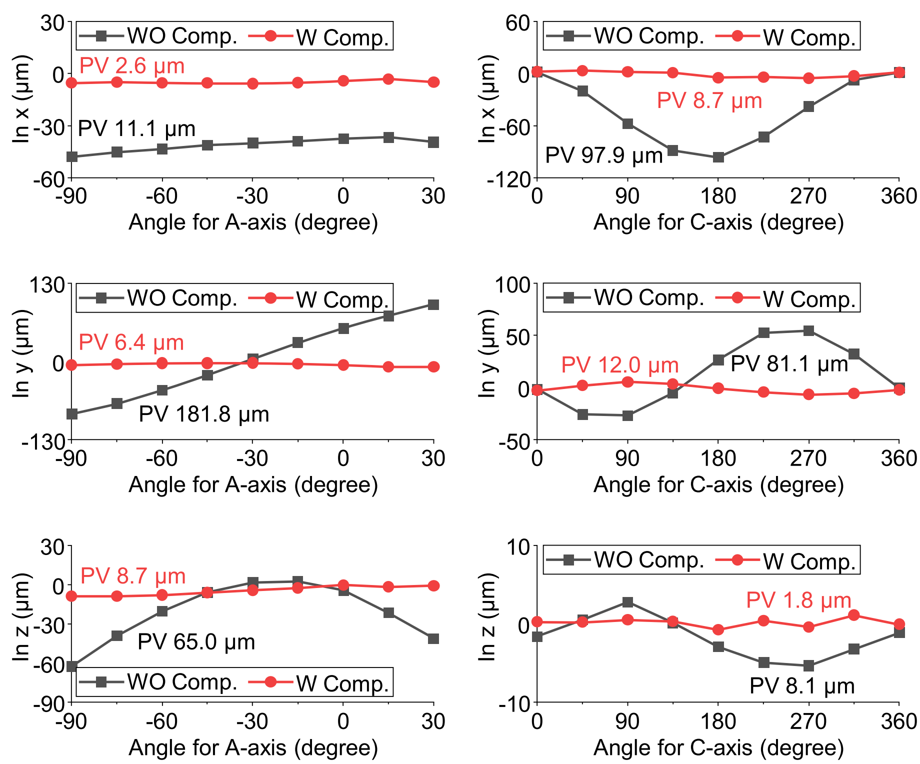

(b) At angle $b = 50°$.

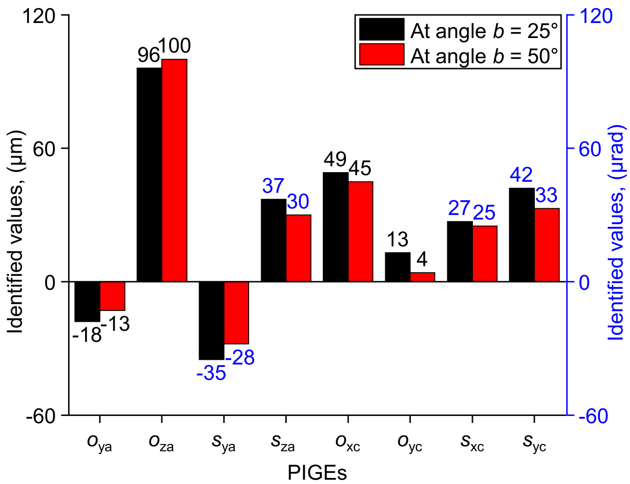

Fig. 13 PIGEs identified at angle b

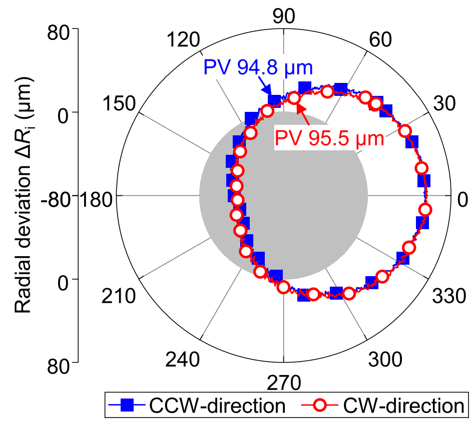

Fig. 15 Measured radial deviations of the DBB measurements (without compensation)

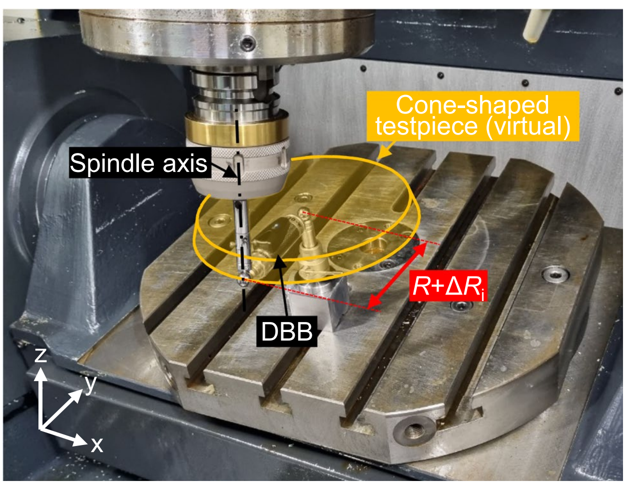

Fig. 14 DBB measurement set-up

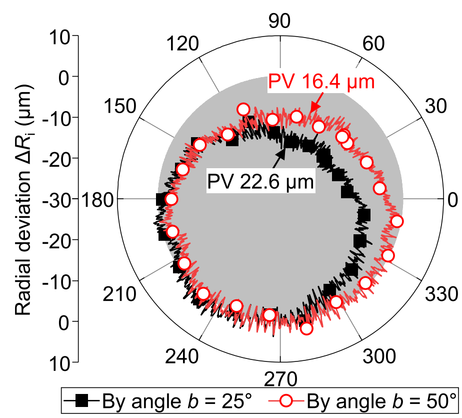

(a) In the CCW direction.

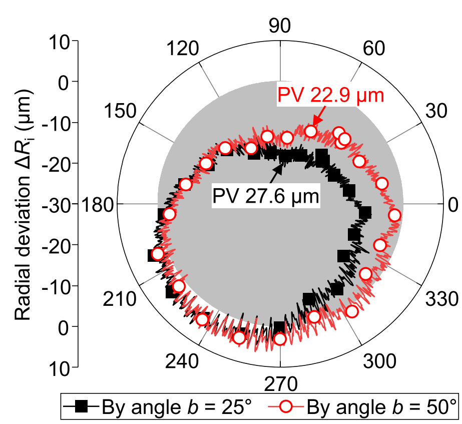

(b) In the CW direction.

Fig. 16 Measured radial deviations of the DBB measurements (with compensation)

(1) To determine the PIGEs of rotary axes, ISO 10791-6 recognizes several methods using a DBB, R-test device, and touch-trigger probe, and defines the test conditions. Most approaches use PIGE measurements to reduce the volumetric errors of machine tools to, in turn, reduce workpiece geometric errors. However, such approaches are vague and indirect; although the improvements are significant, they are limited. It is essential to optimize the well-known method for PIGE measurements associated with workpiece geometric errors and reduce such errors directly.

(2) An error-budgeting model is essential for calculating the measurement uncertainties of identified PIGEs, which reflect a lack of precise knowledge. Calcu-

lated measurement uncertainties are used to derive the PIGE-measuring capabilities of the various methods. Such approaches focus mainly on the effects of measuring devices, and systematic and non-systematic errors of the controlled axes, on the identified PIGEs. However, PIGE measurement uncertainties are also affected by the measurement path, which therefore cannot be ignored. PIGE measurements should be performed along an optimized path, i.e., a path that minimizes the effect of the RSS values of the PIGE sensitivity coefficients on workpiece geometric errors.

(3) Identification of and compensation for the PIGEs of rotary axes may reduce workpiece geometric errors, because the PIGEs are the most significant errors of five-axis machine tools. Equivalent DBB experiments (without compensation) revealed that the radial deviation values of the ISO 10791-7 cone-shaped testpiece were 94.8 and 95.5 µm in the CCW and CW directions, respectively. However, the radial deviation values improved to 22.6 and 27.6 µm after compensation for the identified PIGEs along a common measurement path. Our strategy proved effective; the radial deviation values improved by 16.4 and 22.9 µm (27% and 17% improvements, respectively) when we adaptively identified and compensated for PIGEs along the optimal measurement path. Our method is also cost-effective. In addition, the improvements could be further increased by measuring and compensating the linear axis geometric errors.

(4) Five-axis machine tools play a significant role in the machining of various complex-shaped workpieces; their application is not limited to the ISO 10791-7 cone-shaped testpiece used as an example in this study. The identification method in ISO 10791-6 should be optimized in terms of workpiece geometric error, to maximize error reduction in a direct manner. This can be done by analyzing the RSS values of the sensitivity coefficients. Measurements can then be optimized merely by adjusting the setting angle of a ball on the workpiece table (or the height of the ball from the table), without changing any methods of ISO 10791-6.

Acknowledgements This work was supported by the National Research Foundation of Korea (NRF) grant funded by the Korea government (MSIT) (No.NRF-2023R1A2C2003189).

Declarations

Competing interests The authors declare that they have no conflict of interest.

References

1. Barakat, N. A., Elbestawi, M. A., & Spence, A. D. (2000). Kinematic and geometric error compensation of a coordinate measuring machine. *International Journal of Machine Tools and Manufacture, 40*, 833–850. https://doi.org/10.1016/S0890-6955(99)00098-X
2. Fan, J., Tao, H., Pan, R., & Chen, D. (2020). Optimal tolerance allocation for five–axis machine tools in consideration of deformation caused by gravity. *The International Journal of Advanced Manufacturing Technology, 111*, 13–24. https://doi.org/10.1007/s00170-020-06096-x
3. Gomez-Acedo, E., Olarra, A., Orive, J., & Lopez de la Calle, L. N. (2013). Methodology for the design of a thermal distortion compensation for large machine tools based in state–space representation with Kalman filter. *International Journal of Machine Tools and Manufacture, 75*, 100–108. https://doi.org/10.1016/j.ijmachtools.2013.09.005
4. Schwenke, H., Knapp, W., Haitjema, H., Weckenmann, A., Schmitt, R., & Delbressine, F. (2008). Geometric error measurement and compensation of machines—An update. *CIRP Annals, 57*, 660–675. https://doi.org/10.1016/j.cirp.2008.09.008
5. Ibaraki, S., & Knapp, W. (2012). Indirect measurement of volumetric accuracy for three-axis and five-axis machine tools: A review. *International Journal of Automation Technology, 6*, 110–124. https://doi.org/10.20965/ijat.2012.p0110
6. ISO 230-1. (2012). Test code for machine tools—Part 1: Geometric accuracy of machines operating under no—Load or Quasi–static Conditions. *ISO*.
7. Uddin, M. S., Ibaraki, S., Matsubara, A., & Matsushita, T. (2009). Prediction and compensation of machining geometric errors of five-axis machining centers with kinematic errors. *Precision Engineering, 33*, 194–201. https://doi.org/10.1016/j.precisioneng.2008.06.001
8. Lee, K. I., Lee, D. M., & Yang, S. H. (2012). Parametric modeling and estimation of geometric errors for a rotary axis using double ball-bar. *The International Journal of Advanced Manufacturing Technology, 62*, 741–750. https://doi.org/10.1007/s00170-011-3834-0
9. Lee, K. I., & Yang, S. H. (2016). Compensation of position-independent and position-dependent geometric errors in the rotary axes of five–axis machine tools with a tilting rotary table. *The International Journal of Advanced Manufacturing Technology, 85*, 1677–1685. https://doi.org/10.1007/s00170-015-8080-4
10. Yao, Y., Nishizawa, K., Kato, N., Tsutsumi, M., & Nakamoto, K. (2020). Identification method of geometric deviations for multi-tasking machine tools considering the squareness of translational axes. *Applied Sciences, 10*, 1811. https://doi.org/10.3390/app10051811
11. Yang, S. H., & Lee, K. I. (2022). A dual difference method for identification of the inherent spindle axis parallelism errors of machine tools. *International Journal of Precision Engineering and Manufacturing, 23*, 701–710. https://doi.org/10.1007/s12541-022-00653-y
12. Bringmann, B., & Knapp, W. (2009). Machine tool calibration: Geometric test uncertainty depends on machine tool performance. *Precision Engineering, 33*, 524–529. https://doi.org/10.1016/j.precisioneng.2009.02.002
13. Kenno, T., Sato, R., Shirase, K., Natsume, S., & Spaan, H. A. M. (2020). Influence of linear-axis error motions on simultaneous three-axis controlled motion accuracy defined in ISO 10791–6. *Precision Engineering, 61*, 110–119. https://doi.org/10.1016/j.precisioneng.2019.10.011

14. Ibaraki, S., & Yanai, E. (2021). Identification of rotary axis location errors under spindle rotation by using a laser barrier tool measurement system—Experimental comparison with R-test. *Transactions of the Institute of Systems, Control and Information Engineers, 34*, 81–88. https://doi.org/10.5687/iscie.34.81
15. Onishi, S., Ibaraki, S., Kato, T., Yamaguchi, M., & Sugimoto, T. (2022). A self-calibration scheme to monitor long-term changes in linear and rotary axis geometric errors. *Measurement, 196*, 111183. https://doi.org/10.1016/j.measurement.2022.111183
16. Hong, C., Ibaraki, S., & Matsubara, A. (2011). Influence of position-dependent geometric errors of rotary axes on a machining test of cone frustum by five–axis machine tools. *Precision Engineering, 35*, 1–11. https://doi.org/10.1016/j.precisioneng.2010.09.004
17. ISO 10791-7. (2020). Test conditions for machining centres—Part 7: Accuracy of finished test pieces. *ISO*.
18. Li, Z., Sato, R., Shirase, K., & Sakamoto, S. (2021). Study on the influence of geometric errors in rotary axes on cubic-machining test considering the workpiece coordinate system. *Precision Engineering, 71*, 36–46. https://doi.org/10.1016/j.precisioneng.2021.02.011
19. Ibaraki, S., Sawada, M., Matsubara, A., & Matsushita, T. (2010). Machining tests to identify kinematic errors on five-axis machine tools. *Precision Engineering, 34*, 387–398. https://doi.org/10.1016/j.precisioneng.2009.09.007
20. Ibaraki, S., & Ota, Y. (2014). A machining test to calibrate rotary axis error motions of five-axis machine tools and its application to thermal deformation test. *International Journal of Machine Tools and Manufacture, 86*, 81–88. https://doi.org/10.1016/j.ijmachtools.2014.07.005
21. Ibaraki, S., Tsujimoto, S., Nagai, Y., Sakai, Y., Morimoto, S., & Miyazaki, Y. (2018). A pyramid-shaped machining test to identify rotary axis error motions on five-axis machine tools. *The International Journal of Advanced Manufacturing Technology, 94*, 227–237. https://doi.org/10.1007/s00170-017-0906-9
22. Yang, H., Huang, X., Ding, S., Yu, C., & Yang, Y. (2018). Identification and compensation of 11 position-independent geometric errors on five-axis machine tools with a tilting head. *The International Journal of Advanced Manufacturing Technology, 94*, 533–544. https://doi.org/10.1007/s00170-017-0826-8
23. Jiang, Z., Song, B., Zhou, X., Tang, X., & Zheng, S. (2015). On-machine measurement of location errors on five-axis machine tools by machining tests and a laser displacement sensor. *International Journal of Machine Tools and Manufacture, 95*, 1–12. https://doi.org/10.1016/j.ijmachtools.2015.05.004
24. Tsutsumi, M., & Saito, A. (2003). Identification and compensation of systematic deviations particular to 5-axis machining centers. *International Journal of Machine Tools and Manufacture, 43*, 771–780. https://doi.org/10.1016/S0890-6955(03)00053-1
25. Weikert, S. (2004). R-test, a new device for accuracy measurements on five axis machine tools. *CIRP Annals, 53*, 429–432. https://doi.org/10.1016/S0007-8506(07)60732-X
26. Flynn, J. M., Shokrani, A., Vichare, P., Dhokia, V., & Newman, S. T. (2018). A new methodology for identifying location errors in 5-axis machine tools using a single ballbar set-up. *The International Journal of Advanced Manufacturing Technology, 99*, 53–71. https://doi.org/10.1007/s00170-016-9090-6
27. Liu, Y., Wang, M., Xing, W. J., & Zhang, W. H. (2018). Identification of position independent geometric errors of rotary axes for five-axis machine tools with structural restrictions. *Robotics and Computer-Integrated Manufacturing, 53*, 45–57. https://doi.org/10.1016/j.rcim.2018.03.010
28. Lee, K. I., & Yang, S. H. (2013). Measurement and verification of position-independent geometric errors of a five-axis machine tool using a double ball-bar. *International Journal of Machine Tools and Manufacture, 70*, 45–52. https://doi.org/10.1016/j.ijmachtools.2013.03.010
29. Jiang, X., & Cripps, R. J. (2015). A method of testing position independent geometric errors in rotary axes of a five-axis machine tool using a double ball bar. *International Journal of Machine Tools and Manufacture, 89*, 151–158. https://doi.org/10.1016/j.ijmachtools.2014.10.010
30. Wang, Z., Wang, D., Yu, S., Li, X., & Dong, H. (2021). A reconfigurable mechanism model for error identification in the double ball bar tests of machine tools. *International Journal of Machine Tools and Manufacture, 165*, 103737. https://doi.org/10.1016/j.ijmachtools.2021.103737
31. Mayer, J. R. R. (2012). Five–axis machine tool calibration by probing a scale enriched reconfigurable uncalibrated master balls artefact. *CIRP Annals, 61*, 515–518. https://doi.org/10.1016/j.cirp.2012.03.022
32. Ibaraki, S., Iritani, T., & Matsushita, T. (2012). Calibration of location errors of rotary axes on five-axis machine tools by on-the-machine measurement using a touch-trigger probe. *International Journal of Machine Tools and Manufacture, 58*, 44–53. https://doi.org/10.1016/j.ijmachtools.2012.03.002
33. ISO 10791-6. (2014). Test conditions for machining centres—Part 6: Accuracy of speeds and interpolations. ISO.
34. Li, Q., Wang, W., Zhang, J., Shen, R., Li, H., & Jiang, Z. (2019). Measurement method for volumetric error of five-axis machine tool considering measurement point distribution and adaptive identification process. *International Journal of Machine Tools and Manufacture, 147*, 103465. https://doi.org/10.1016/j.ijmachtools.2019.103465
35. Sepahi-Boroujeni, S., Mayer, J. R. R., & Khameneifar, F. (2021). Efficient uncertainty estimation of indirectly measured geometric errors of five-axis machine tools via Monte-Carlo validated GUM framework. *Precision Engineering, 67*, 160–171. https://doi.org/10.1016/j.precisioneng.2020.09.027
36. ISO/IEC Guide 98-3. (2008). Uncertainty of measurement—Part 3: Guide to the expression of uncertainty in measurement (GUM:1995). *ISO*.
37. Yang, S. H., & Lee, K. I. (2021). Identification of 11 Position-independent geometric errors of a five-axis machine tool using 3D geometric sensitivity analysis. *The International Journal of Advanced Manufacturing Technology, 113*, 3271–3282. https://doi.org/10.1007/s00170-021-06844-7
38. Yang, S. H., & Lee, K. I. (2021). Machine tool analyzer: A device for identifying 13 position-independent geometric errors for five-axis machine tools. *The International Journal of Advanced Manufacturing Technology, 115*, 2945–2957. https://doi.org/10.1007/s00170-021-07341-7
39. Zha, J., Wang, T., Li, L., & Chen, Y. (2020). Volumetric error compensation of machine tool using laser tracer and machining verification. *The International Journal of Advanced Manufacturing Technology, 108*, 2467–2481. https://doi.org/10.1007/s00170-020-05556-8
40. ISO 230-7. (2015). Test code for machine tools—Part 7: Geometric accuracy of axes of rotation. *ISO*.
41. Lee, K. I., Lee, J. C., & Yang, S. H. (2018). Optimal on-machine measurement of position-independent geometric errors for rotary axes in five-axis machines with a universal head. *International Journal of Precision Engineering and Manufacturing, 19*, 545–551. https://doi.org/10.1007/s12541-018-0066-3
42. Lee, K. I., & Yang, S. H. (2014). Circular tests for accurate performance evaluation of machine tools via an analysis of eccentricity. *International Journal of Precision Engineering and Manufacturing, 15*, 2499–2506. https://doi.org/10.1007/s12541-014-0620-6
43. ISO 230-4. (2022). Test code for machine tools—Part 4: Circular tests for numerically controlled machine tools. *ISO*.

Seung-Han Yang received the Ph.D. degree in mechanical engineering from the University of Michigan, Ann Arbor, Michigan, USA. He is currently a professor in the School of Mechanical Engineering, Kyungpook National University. His research interest is intelligent manufacturing systems and CAD/CAM.

Kwang-Il Lee received the Ph.D. degree in mechanical engineering from the Kyungpook National University, Daegu, Republic of Korea. He is currently a professor in the School of Mechanical and Automotive Engineering, Kyungil University. His research interest is precision methodologies for machine tools, precision robots, and 3D printers.